JCI insight

The ribosomal prolyl-hydroxylase OGFOD1 decreases during cardiac differentiation and modulates translation and splicing

Andrea Stoehr, … , Jizhong Zou, Elizabeth Murphy

JCI Insight. 2019;4(13):e128496. https://doi.org/10.1172/jci.insight.128496.

Research Article Cardiology

The mechanisms regulating translation and splicing are not well understood. We provide insight into a new regulator of translation, 2-oxoglutarate and iron dependent oxygenase domain–containing protein 1 (OGFOD1), which is a prolyl-hydroxylase that catalyzes the posttranslational hydroxylation of Pro62 in the small ribosomal protein S23. We show that deletion of OGFOD1 in an in vitro model of human cardiomyocytes decreases translation of specific proteins (e.g., RNA-binding proteins) and alters splicing. RNA-Seq showed poor correlation between changes in mRNA and protein synthesis, suggesting that posttranscriptional regulation was the primary cause for the observed differences. We found that loss of OGFOD1 and the resultant alterations in protein translation modulated the cardiac proteome, shifting it toward higher protein amounts of sarcomeric proteins, such as cardiac troponins, titin, and cardiac myosin-binding protein C. Furthermore, we found a decrease of OGFOD1 during cardiomyocyte differentiation. These results suggest that loss of OGFOD1 modulates protein translation and splicing, thereby leading to alterations in the cardiac proteome, and highlight the role of altered translation and splicing in regulating the proteome.

JCI insight

RESEARCH ARTICLE

The ribosomal prolyl-hydroxylase OGFOD1 decreases during cardiac differentiation and modulates translation and splicing

Andrea Stoehr,[1] Leslie Kennedy,[1] Yanqin Yang,[2] Sajni Patel,[3] Yongshun Lin,[4] Kaari L. Linask,[4] Maria Fergusson,[1] Jun Zhu,[2] Marjan Gucek,[3] Jizhong Zou,[4] and Elizabeth Murphy[1]

[1]Cardiovascular Branch, [2]DNA Sequencing and Genomics Core, [3]Proteomics Core Facility, and [4]iPS Cell Core Facility, National Heart, Lung, and Blood Institute, NIH, Bethesda, Maryland, USA.

The mechanisms regulating translation and splicing are not well understood. We provide insight into a new regulator of translation, 2-oxoglutarate and iron dependent oxygenase domain–containing protein 1 (OGFOD1), which is a prolyl-hydroxylase that catalyzes the posttranslational hydroxylation of Pro62 in the small ribosomal protein S23. We show that deletion of OGFOD1 in an in vitro model of human cardiomyocytes decreases translation of specific proteins (e.g., RNA-binding proteins) and alters splicing. RNA-Seq showed poor correlation between changes in mRNA and protein synthesis, suggesting that posttranscriptional regulation was the primary cause for the observed differences. We found that loss of OGFOD1 and the resultant alterations in protein translation modulated the cardiac proteome, shifting it toward higher protein amounts of sarcomeric proteins, such as cardiac troponins, titin, and cardiac myosin-binding protein C. Furthermore, we found a decrease of OGFOD1 during cardiomyocyte differentiation. These results suggest that loss of OGFOD1 modulates protein translation and splicing, thereby leading to alterations in the cardiac proteome, and highlight the role of altered translation and splicing in regulating the proteome.

Introduction

Although changes in translation and altered splicing play an important role in differentiation and disease processes, such as cancer and heart failure (1–6), the precise mechanisms regulating them are not well understood. In this manuscript we provide insight into a new regulator of translation, 2-oxoglutarate and iron dependent oxygenase domain–containing protein 1 (OGFOD1). Protein prolyl-hydroxylases are a family of enzymes dependent on oxygen and α-ketoglutarate that catalyze hydroxylation of amino acid residues, such as prolines or asparagines (7–9). We examined the role of a newly described ribosomal prolyl-hydroxylase, OGFOD1. OGFOD1 has been shown to hydroxylate a proline (P62) in the ribosomal protein S23 (Rps23), which regulates translation, and inhibition of OGFOD1 has been reported to lead to a decrease in translation and an increase in stress granule formation (10, 11). The precise role of OGFOD1 in human cardiomyocytes is unclear. In addition, inhibitors of the HIF prolyl-hydroxylase (prolyl-hydroxylase domain–containing protein 2, PHD2), which are currently in clinical trials to treat anemia, have also been recently shown to inhibit OGFOD1, adding to the importance of understanding the role of OGFOD1 (12).

To better define the specific role of OGFOD1, we deleted OGFOD1 and compared protein synthesis, stability, and levels in isogenic WT and OGFOD1-knockout induced pluripotent stem cell–derived cardiomyocytes (OGFOD1-KO iPSC-CMs). We used a previously developed in vitro model of human iPSC-CMs (13) in which we used CRISPR/Cas9 to delete OGFOD1. In vitro models of human stem cell–derived cardiomyocytes have become important for a wide range of biomedical applications, such as disease modeling and drug screening (14–16). We found that loss of OGFOD1 led to a decrease in protein synthesis in proteins enriched in ribosomal proteins and splicing factors, consistent with an important role for OGFOD1 in regulating protein translation. When comparing the proteomic profiles of OGFOD1-KO with WT iPSC-CMs, we made the surprising finding that loss of OGFOD1 led to an increase in a number of cardiac-specific proteins. These data are consistent with the hypothesis that OGFOD1 alters translation of specific proteins, leading to an altered protein landscape, thus accelerating cardiac differentiation and enhancing the

Conflict of interest: The authors have declared that no conflict of interest exists.

Submitted: March 4, 2019
Accepted: May 16, 2019
Published: July 11, 2019.

Reference information: *JCI Insight*. 2019;4(13):e128496. https://doi.org/10.1172/jci.insight.128496.

levels of cardiac proteins at day 16 after initiation of differentiation. Several recent studies have reported that changes in translation and altered splicing play an important role in cardiac differentiation. However, the precise mechanisms regulating these alterations in translation and splicing are not well understood. In this manuscript, we provide insight into a new regulator of translation and splicing, OGFOD1.

Results

Loss of OGFOD1 remodels the proteome. To characterize the role of OGFOD1 in human iPSC-CMs, we performed quantitative proteomics on WT and OGFOD1-KO iPSC-CMs to identify potential differences in total protein levels. Differences detected in the proteomic profiles between OGFOD1-KO and WT are illustrated in the heatmap analysis depicting distinct clustering of WT and OGFOD1-KO and in the volcano plot analysis (Figure 1, A and B, and Supplemental Figure 1, A and B; supplemental material available online with this article; https://doi.org/10.1172/jci.insight.128496DS1). As shown in the volcano plot (Figure 1B), we observed a similar distribution of proteins with increased (207 proteins) and decreased (169 proteins) levels in OGFOD1-KO compared with WT (cutoff ± 30%; $P < 0.05$; Supplemental Table 1). Of note, a large number of ribosomal proteins exhibited a decrease in OGFOD1-KO (highlighted in orange Figure 1B). To further characterize differences in the cardiac proteome between OGFOD1-KO and WT, we subjected the proteins showing a significant difference to gene ontology analysis using DAVID software. We found that translational initiation, cell-cell adhesion, and mRNA splicing via spliceosome were decreased in abundance in OGFOD1-KO (Figure 1C). OGFOD1-KO showed higher abundance in glycolytic processes, TCA cycle, and cardiac muscle contraction (Figure 1D). Analyzing the proteomic changes, we noted that loss of OGFOD1 resulted in a significant increase in sarcomeric proteins, such as titin; cardiac troponins T, C, and I; sarcoplasmic/endoplasmic reticulum calcium transporter (SERCA2A; ATP2A2); sodium-calcium exchanger (NCX; SLC8A1); and cardiac myosin-binding protein C (MYBPC3; Figure 1E). In addition, myosin and titin interacting protein myomesin 1 (MYOM1) and a muscle-specific creatinine kinase were increased in OGFOD1-KO. The increase in markers of cardiac differentiation in the OGFOD1-KO iPSC-CMs might suggest that OGFOD1 has an inhibitory effect on cardiomyocyte differentiation and that its repression enhances or accelerates cardiomyocyte differentiation. Consistent with this hypothesis, we found that OGFOD1 mRNA (Figure 1F) and protein expression (Figure 1G) decreased at the onset of cardiomyocyte differentiation. We also measured Brachyury and mesoderm posterior bHLH transcription factor 1 (MESP1) to determine how OGFOD1 deletion affects the early stages of cardiomyocyte differentiation. As shown in Figure 1H, during the initial 48 hours of differentiation, Brachyury is upregulated to peak at 12 hours and downregulated beyond the 12-hour time point more rapidly in OGFOD1-KO cells than in WT cells. Additionally, Brachyury levels at the 12-hour time point are significantly higher in OGFOD1-KO cells. We also find that at 48 hours of differentiation, MESP1 levels are higher in OGFOD1-KO cells than WT cells (Figure 1I). Altogether, these data suggest OGFOD1-KO cells achieve mesoderm and cardiogenic mesoderm fates more robustly and more rapidly than WT cells, further supporting a role for OGFOD1 in repressing cardiomyocyte differentiation.

OGFOD1 affects protein synthesis and degradation in human cardiomyocytes. We further examined the mechanisms responsible for the differences in the proteomic profiles observed between OGFOD1-KO and WT. Because OGFOD1 is known to influence translation (10), we hypothesized that there might be differences in protein synthesis in OGFOD1-KO versus WT cardiomyocytes. To address this hypothesis, we used a previously developed labeling method in iPSC-CMs (17). We cultured OGFOD1-KO and WT cardiomyocytes in media containing light amino acids and then switched them to media containing heavy amino acids and followed the incorporation of the heavy label as a measure of protein synthesis and the loss of the light label as a measure of protein degradation. After 24 hours of labeling, 128 proteins exhibited a significant decrease, and 1 protein showed a significant increase in protein synthesis in OGFOD1-KO in comparison with WT (Figure 2A and Supplemental Table 2). A comparison to the proteomics data showed that of the 128 proteins in OGFOD1-KO with decreased protein synthesis, 70 also exhibited a decrease in the level of the protein, suggesting that the decrease in protein synthesis plays a role in the changes observed in the total protein level for these proteins. We performed PANTHER (protein analysis through evolutionary relationships) protein class analysis on the proteins, which exhibited a significant decrease in protein synthesis in OGFOD1-KO iPSC-CMs, and found enrichment in proteins annotated to cytoskeletal proteins, nucleic acid–binding proteins, and chaperones (Figure 2B). In the cytoskeletal protein pathway, primarily the actin family showed a decrease in protein synthesis. For nucleic acid–binding proteins, most of the affected

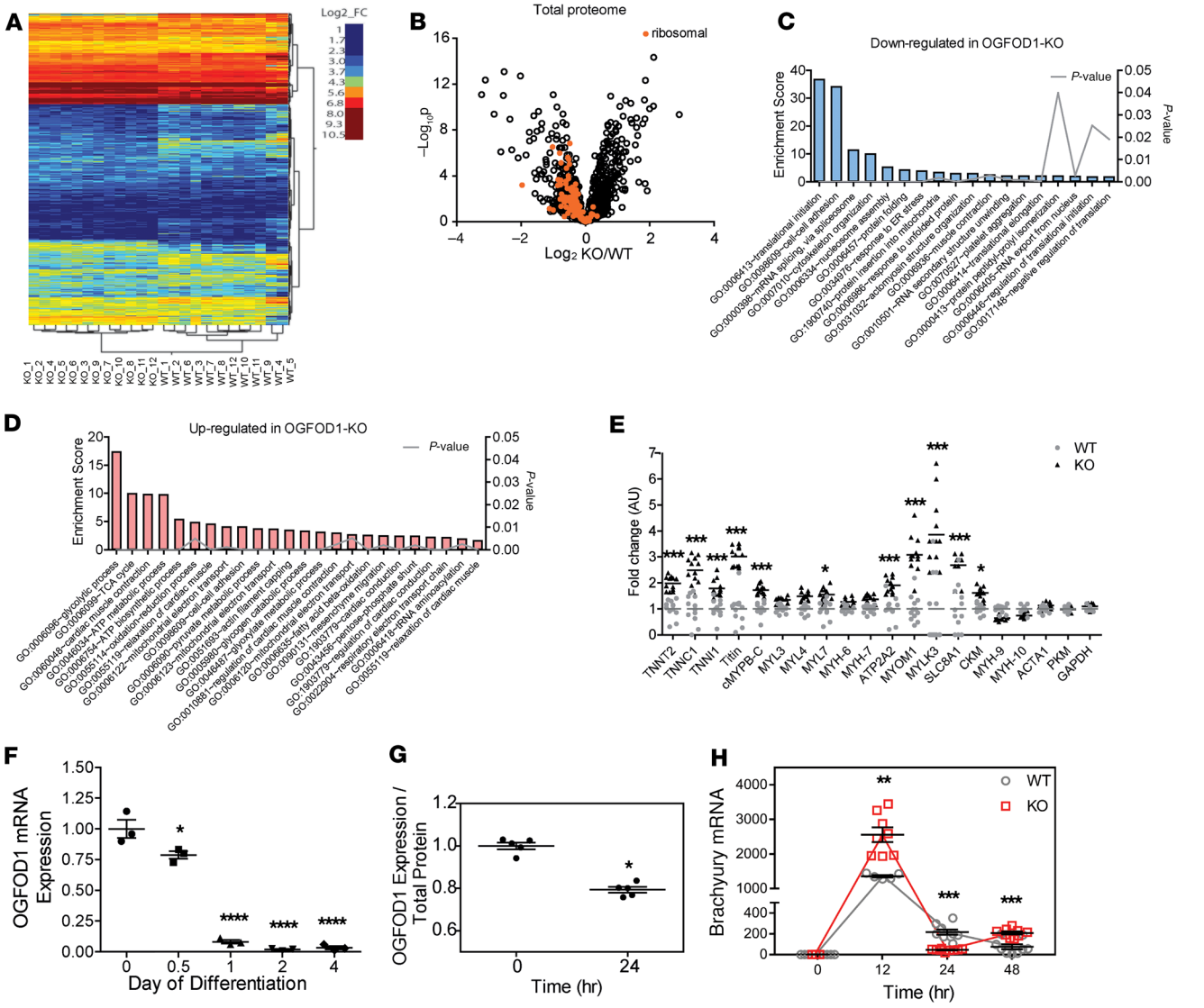

Figure 1. Quantitative analyses of proteomic profiles and differentiation status of WT and OGFOD1-KO iPSC-CMs. (**A**) Cluster analysis shows a clear difference between the proteomic profiles of KO and WT. The level of each protein is shown in rows, and samples are clustered in columns. The protein levels across the samples are shown as $\log_2$ counts per million (CPM). The scaled expression values are color coded according to the legend. FC, fold change. (**B**) Volcano plot to compare the mean $\log_2$FCs (OGFOD1-KO/WT) of normalized spectral counts and the $\log_{10}$ of the *P* values obtained in the *t* test comparison. Protein classes are highlighted for ribosomal proteins. Gene ontology analysis was performed with Database for Annotation, Visualization and Integrated Discovery (DAVID) software for biological processes being enriched for proteins that were significantly lower in OGFOD1-KO (**C**) and for proteins that were significantly higher in OGFOD1-KO (**D**), respectively. (**E**) Differences in protein levels between WT and OGFOD1-KO for proteins associated with cardiomyocyte maturation. $n = 12$ per group. (**F**) Changes in OGFOD1 expression for various time points following initiation of differentiation in iPSCs. $n = 3$ per time point. (**G**) Changes in OGFOD1 protein level in iPSCs during cardiac differentiation, normalized on total protein amount. $n = 5$ per time point. Development of cardiac differentiation marker genes, such as Brachyury (**H**) and Mesp1 (**I**), over a cardiac differentiation period of 48 hours. $n = 8$ per time point. Data are shown as mean ± SEM. $^{***}P < 0.001$ and $^{*}P < 0.05$ vs. WT (2-way ANOVA plus Bonferroni's posttest) in **E**. $^{****}P < 0.0001$ and $^{*}P < 0.05$ vs. day 0 (1-way ANOVA plus Bonferroni's posttest) in **F**. $^{*}P < 0.05$ vs. time point 0 (Student's *t* test) in **G**. $^{****}P < 0.0001$, $^{***}P < 0.001$, and $^{**}P < 0.01$ vs. day 0 (2-way ANOVA plus Bonferroni's posttest) in **H** and **I**.

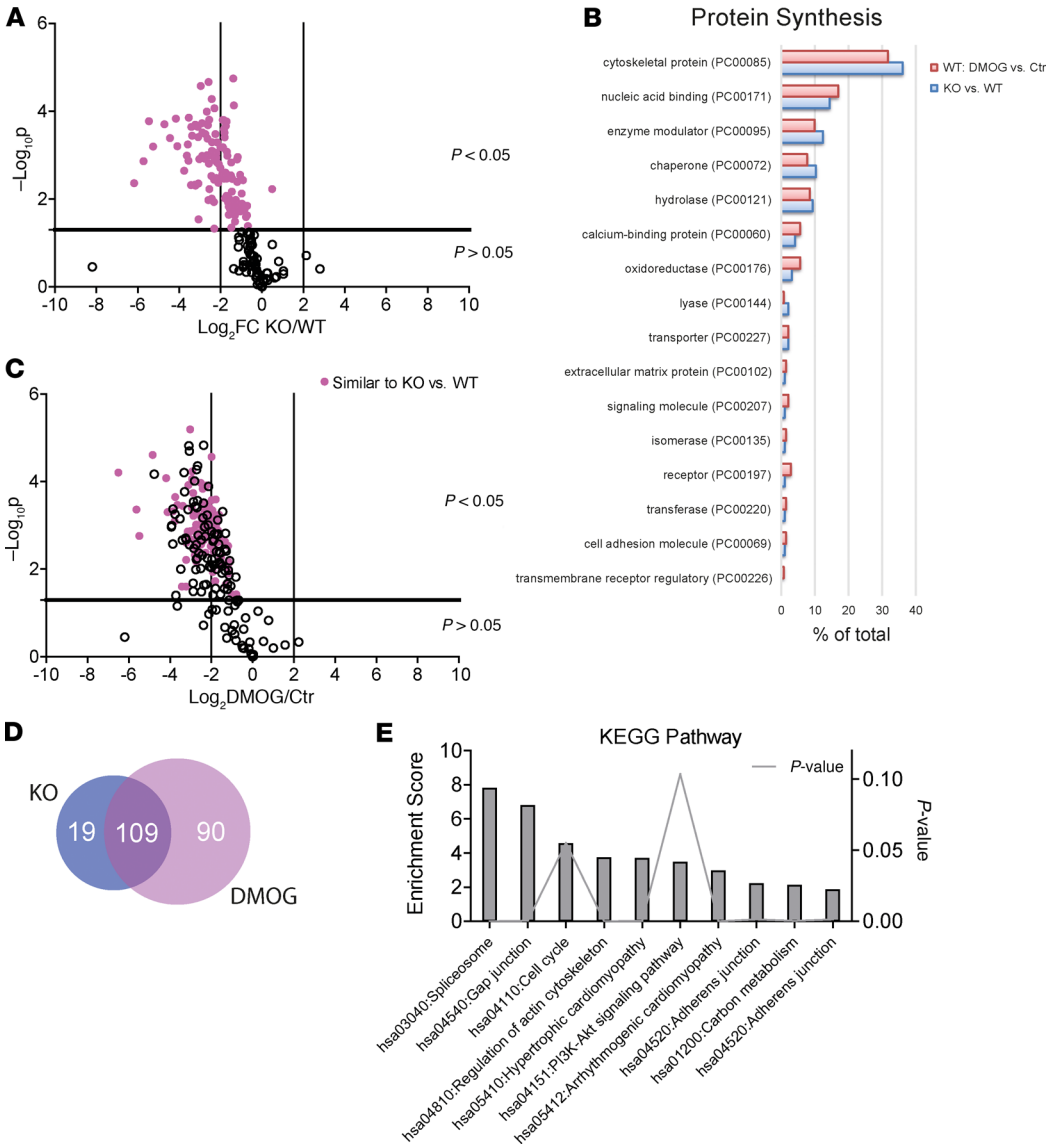

Figure 2. Analysis of incorporated heavy amino acid label into WT and OGFOD1-KO iPSC-CMs as a measure of protein synthesis. Human iPSC-CMs were analyzed 16 days after initiation of the differentiation. Cardiomyocytes were adapted to dialyzed FBS containing light medium ($^{12}C_6$–Lys, $^{12}C_6{}^{14}N_4$–Arg) for 3 days and then switched to heavy label ($^{13}C_6$ L-lysine-2HCl, $^{13}C_6{}^{15}N_4$ L-arginine-HCl). For the analysis of protein stability, samples were harvested 24 hours after media switch. Samples underwent tryptic digestion and mass spectrometry analysis. Quantitative analysis was performed by QUOIL (QUantification withOut Isotope Labeling). (**A**) Volcano plot analysis for heavy proteins showing basal differences in protein synthesis in KO vs. WT. $n = 3$ biological samples per group. (**B**) Protein class analysis was performed for proteins with significant differences in protein synthesis with PANTHER. Protein classes are shown as percentage of total number of identified protein classes. (**C**) Volcano plot analysis for heavy proteins showing basal differences in protein synthesis in WT Ctr versus dimethyloxalylglycine (DMOG, 1 mM). $n = 3$ biological samples per group. (**D**) Venn diagram overlap of proteins with significant differences in protein synthesis in OGFOD1-KO vs. WT and WT ± DMOG. (**E**) KEGG pathway enrichment analysis was performed with DAVID showing pathways for common proteins with decrease in synthesis. Volcano plots: The horizontal line represents the threshold of $P = 0.05$; the vertical lines represent the threshold for the $\log_2$FC. The x axis depicts the $\log_2$ difference in protein synthesis.

proteins were RNA-binding proteins. Because OGFOD1 is deleted in germline, we compared the proteins that showed a decrease in translation in OGFOD1-KO iPSC-CMs to the proteins that showed a decrease in protein synthesis with acute addition of dimethyloxalylglycine (DMOG) and found that approximately 85% of the proteins showing a significant decrease in protein synthesis in OGFOD1-KO also showed a significant decrease in WT plus DMOG (Figure 2, A and C). Thus, the overall decrease in protein synthesis

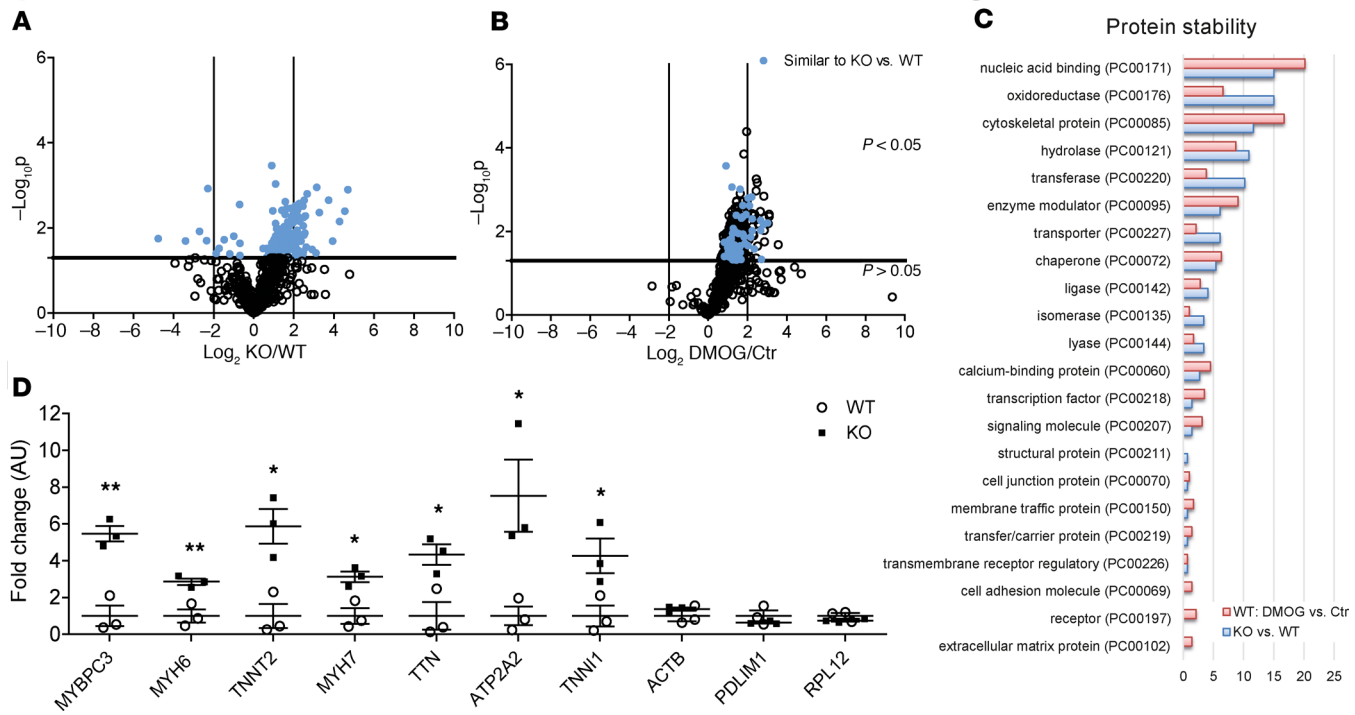

Figure 3. Analysis of light proteins in pulse-chase amino acid–labeled WT and OGFOD1-KO iPSC-CMs. Human iPSC-CMs were analyzed 16 days after initiation of the differentiation. Cardiomyocytes were adapted to dialyzed FBS containing light medium ($^{12}C_6$–Lys, $^{12}C_6{}^{14}N_4$–Arg) for 3 days and then switched to heavy label ($^{13}C_6$ L-lysine-2HCl, $^{13}C_6{}^{15}N_4$ L-arginine-HCl). For the analysis of protein degradation, samples were harvested 6 hours after media switch. Samples underwent tryptic digestion and mass spectrometry analysis. Quantitative analysis was performed by QUOIL. Volcano plot analysis for light proteins showing basal differences in protein degradation in OGFOD1-KO versus WT (**A**) or WT Ctr versus DMOG (1 mM) (**B**), with $n = 3$ biological samples per group. The horizontal line represents the threshold of $P = 0.05$; the vertical lines represent the threshold for the $\log_2$FC. The x axis depicts the $\log_2$ difference in protein synthesis. (**C**) Protein class analysis was performed for proteins with significant differences in protein synthesis with PANTHER. Protein classes are shown as percentage of total number of identified protein classes. (**D**) Protein stability for selected cardiac proteins undergoing stabilization versus selected proteins without significant changes in protein stability at different time points after initiation of labeling. Data are shown as mean ± SEM. $^{**}P < 0.01$ and $^{*}P < 0.05$ vs. WT (2-way ANOVA plus Bonferroni's posttest).

that we observed with addition of DMOG is largely explained by inhibition of OGFOD1. We reasoned that the overlapping proteins would reveal proteins acutely regulated by a decrease in OGFOD1. For the 109 overlapping proteins showing a significant decrease in protein synthesis in OGFOD1-KO as well as in WT DMOG (Figure 2D), enrichment analysis with DAVID software revealed that most of these were associated with the spliceosome Kyoto Encyclopedia of Genes and Genomes (KEGG) pathway (Figures 2E).

We also investigated differences in protein degradation in OGFOD1-KO versus WT by quantifying the loss of the light amino acid label 6 hours after the cells were switched into heavy-labeled amino acids (Figure 3A). This time point was chosen because the light label is largely lost by 24 hours in proteins that turn over rapidly. After 6 hours, 184 proteins were significantly different in OGFOD1-KO versus WT, and approximately 93% of these exhibited stabilization in OGFOD1-KO (Figure 3A and Supplemental Table 3). Again, we further compared these results to the response to an overall inhibition of prolyl-hydroxylases with DMOG and found overlapping proteins as depicted in Figure 3B. When we subjected proteins showing an increase in protein stability in OGFOD1-KO versus WT and WT DMOG versus control to PANTHER protein class analysis, these proteins were mainly nucleic acid–binding proteins, cytoskeletal proteins, and oxidoreductases (Figure 3C). Interestingly, for the cytoskeletal proteins, mainly proteins within the actin family showed an increase in protein stability; this is the same protein class identified for proteins with significant decreases in protein synthesis. The same phenomenon was observed for nucleic acid–binding proteins as a class, which exhibited a decrease in protein synthesis and an increase in protein stability. Proteins in the same pathways showed both an increase in stability and a decrease in synthesis; these changes would oppose one another if they occurred on the same protein. However, if they occurred on different proteins in the pathway, it would be a way of altering the specific protein composition and rewiring a pathway. A careful examination of these proteins showed that different proteins in a pathway were stabilized compared with

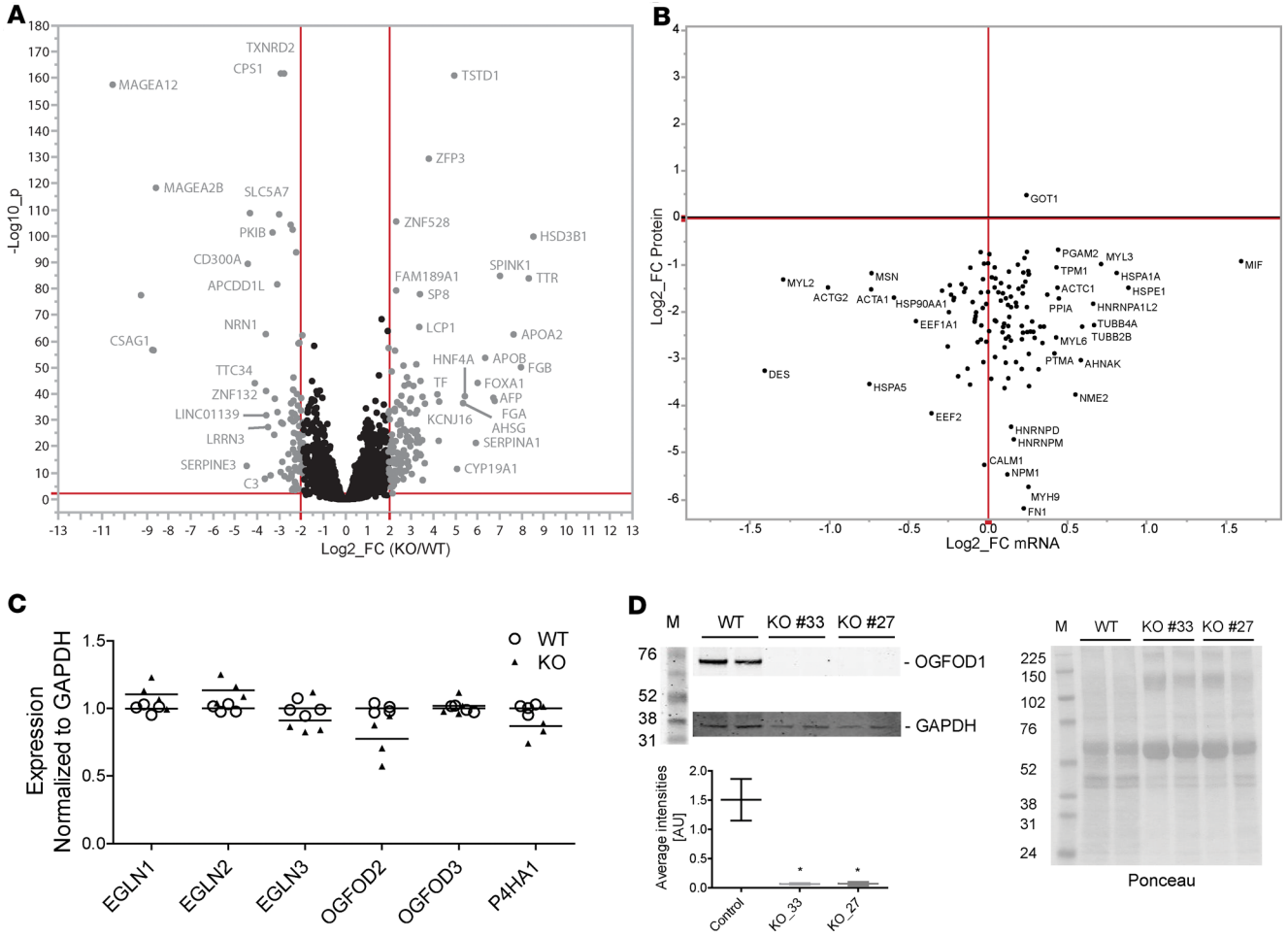

Figure 4. Comparison of the cardiac transcriptome obtained by RNA-Seq and protein translation and confirmation of OGFOD1 knockout. (**A**) Volcano plot of RNA-Seq data of basic differences between ODFOD1-KO versus WT cardiomyocytes. *n* = 4 per group. The horizontal line represents the false positive control (FDR) at 1%; the vertical lines represent the threshold for the $\log_2$FC. The *x* axis depicts the $\log_2$ difference in estimated relative expression values. Vertical lines represent the threshold for the $\log_2$FC. Transcripts upregulated (right) or downregulated (left) that are changed greater than 4-fold are highlighted in gray. (**B**) Correlation between differences in proteins (heavy) and mRNA synthesis shows the basic differences between ODFOD1-KO and WT. The red lines highlight the zero value. (**C**) Gene expression (mRNA) of other oxygen-dependent oxygenases, such as EGLN1, EGLN2, EGLN3, OGFOD3, OGFOD2, and P4HA1, in OGFOD1-KO versus WT. (**D**) Western blot analysis to analyze protein levels of OGFOD1 in different clones in comparison to GAPDH and to Ponceau. *n* = 2 per group. Data are shown as mean ± SEM. **P* < 0.05 vs. control/WT (1-way ANOVA plus Bonferroni's posttest).

those with decreased translation. For example, in OGFOD1-KO there was a decrease in protein synthesis in myosin heavy chain 9 (MYH9) and myosin light chain 2, 6, and 9 (MYL2, MYL6, MYL9) and an increase in stability in MYBPC3, myosin heavy chain 6 and 7 (MYH6, MYH7), myosin light chain 4 and 7 (MYL4, MYL7), and MYOM1. Similarly, for RNA-binding proteins there was a decrease in protein synthesis of heterogenous nuclear ribonucleoprotein (hnRNP) A1, hnRNPAIL2, hnRNPA2B1, hnRNPAB, hnRNPC, hnRNPD, hnRNPH1, hnRNPK, hnRNPM, and hnRNPU and an increase in stability of hnRNPA3 and hnRNPH3 (Supplemental Tables 2 and 3). These changes suggest an alteration of the isoform expression of contractile proteins and nucleic acid–binding proteins in OGFOD1-KO. Figure 3D depicts increases in protein stability in various cardiac proteins.

OGFOD1 modifies the cardiac transcriptome and causes a deficit in translation. We further performed RNA-Seq to investigate whether there are differences in the cardiac transcriptome between OGFOD1-KO and WT iPSC-CMs and to determine whether the observed differences in protein synthesis are due to transcriptional or translational changes. The volcano plot in Figure 4A shows the differences in mRNA transcripts between OGFOD1-KO and WT under basal conditions with an even distribution between up- and downregulated transcripts. Gene ontology analysis for differentially expressed transcripts revealed that OGFOD1-KO upregulated processes included mitochondrial respiration and ATP synthesis, as well

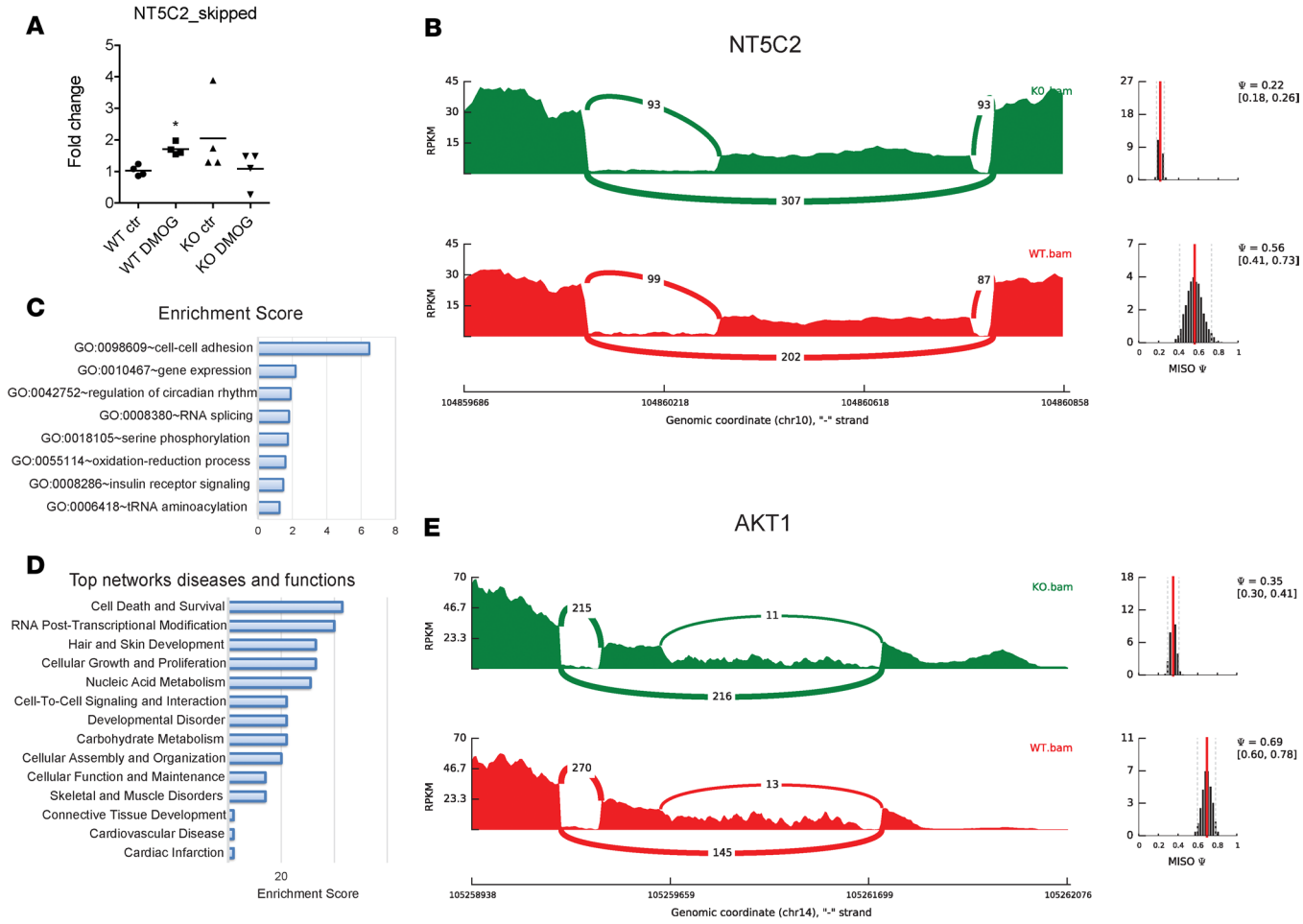

Figure 5. Quantitative reverse transcription PCR and MISO analysis for RNA-Seq data in WT and OGFOD1-KO iPSC-CMs. (**A**) Quantitative PCR analysis was performed for a gene that was previously identified to show differences in alternative splicing between Ctr and DMOG. mRNA transcripts for the exon-skipped variant of NT5C2 were quantified in OGFOD1-KO versus WT (n = 4 per group, normalization to cDNA amount). Data are shown as means ± SEM. *P < 0.05 vs. WT Ctr (Student's t test). (**B**) MISO analysis of WT and OGFOD1-KO was performed from the RNA-Seq data and was able to identify NT5C2 as being significantly different in exon skipping in OGFOD1-KO. (**C**) Gene ontology analysis performed with DAVID for MISO genes that were significantly different for exon skipping. (**D**) IPA network analysis was performed for genes that were identified as being significantly different between OGFOD1-KO and WT. Note that the top 2 networks are cell death and survival and RNA posttranscriptional modification. (**E**) An example for a gene (AKT1) that regulates cell survival and was identified as being significantly different in exon skipping in OGFOD1-KO versus WT identified by MISO analysis.

as cardiac tissue morphogenesis, whereas translational processes were downregulated in OGFOD1-KO (Supplemental Table 4). We analyzed the correlation between differentially expressed mRNA transcription and differences in protein synthesis between OGFOD1-KO and WT and found a poor correlation (Figure 4B), which suggests that posttranscriptional regulations were primarily responsible for the observed differences. Interestingly, this matches previous findings of the effect of DMOG in cardiomyocytes and could be verified again in this study (Supplemental Figure 2). In OGFOD1-KO we found a significant decrease in translation of 128 proteins, and only 16 of these proteins showed a corresponding decrease in mRNA. In fact, the mRNA levels were increased for 49 of the 128 proteins, showing a decrease in translation. We examined the transcriptomics data set to determine whether there was a potential compensatory response, but transcript levels of other related proline oxygenases, such as EGLN1 (Egl-9 family HIF 1, also known as PHD2) and OGFOD3, were unaffected in OGFOD1-KO (Figure 4C). Western blot analysis confirmed a lack of OGFOD1 at the protein level in different clones, when compared with GAPDH (Figure 4D). The Ponceau stain showed other proteins in OGFOD1-KO clones were still abundantly expressed.

Knockout of the ribosomal hydroxylase OGFOD1 influences alternative splicing. As mentioned above, we found 128 proteins with a decrease in translation in OGFOD1-KO, and 112 of these proteins showed either no change or an increase in mRNA; thus, the decrease in translation of these proteins was not due

Table 1. Prolyl hydroxylated peptides and their annotated proteins detected only in WT but not in OGFOD1-KO

No.	Label	Description	Protein accession	Peptide sequences
1	**Light**	**40S ribosomal protein S11**	**P62280**	DVQIGDIVTVGECR***p***LSK
2	**Light**	**40S ribosomal protein S23**	**P62266**	VGVEAKQ***p***NSAIR
3	**Light**	**Arf-GAP with SH3 domain, ANK repeat and PH domain–containing protein 2**	**O43150**	K***p***A***p***GADKST***p***LTNKGQ***p***R
4	**Light**	**Cytochrome b-c1 complex subunit 1, mitochondrial**	**P31930**	ADLTEYLSTHYKA***p***R
5	Light	Drebrin	Q16643	MA***p***T***p***I***p***TRS***p***SDSSTASTPVAEQIER
6	**Light**	**Eukaryotic translation initiation factor 5A-1**	**P63241**	YEDICPSTHNMDV***p***NIKR
7	Light	Filamin-A	P21333	DAGEGLLAVQITD***p***EGK***p***K, ALGALVDSCAPGLCPDWDSWDASK***p***VTNAR
8	Light	Heat shock cognate 71 kDa protein	P11142	HWPFMVVNDAGR***p***K
9	Light	Heterogeneous nuclear ribonucleoprotein M	P52272	GIGTVTFEQSIEAVQAISMFNGQLLFDR***p***MHVK
10	Light	High mobility group protein HMGI-C	P52926	GEGAGQPSTSAQGQPAAPA***p***QKR
11	**Light**	**Histone-binding protein RBBP7**	**Q16576**	TPSSDVLVFDYTKH***p***AKPDPSGECNPDLR
12	Light	Melanoma-associated antigen D2	Q9UNF1	AQETEAAPSQAPADEPEPESAAAQSQENQDTR***p***K
13	Light	Myosin light polypeptide 6	P60660	VLDFEHFL***p***MLQTVAK
14	Light	Nucleophosmin	P06748	MSVQ***p***TVSLGGFEITPPVVLR
15	**Light**	**Phosphatidate phosphatase LPIN2**	**Q92539**	GTIL***p***R
16	Light	Thioredoxin domain–containing protein 5	Q8NBS9	HLYTADMFTHGIQSAAHFVMFFA***p***WCGHCQR
17	**Light**	**Tubulin beta-6 chain**	**Q9BUF5**	IREEF***p***DRIMNTFSVMPSPK
1	Heavy	Alpha-actinin-4	O43707	LMLLLEVISGERL***p***KPER
2	**Heavy**	**Arachidonate 5-lipoxygenase**	**P09917**	QL***p***AVH***p***IFK
3	Heavy	Barrier-to-autointegration factor	O75531	TTSQKHRDFVAE***p***MGEKPVGSLAGIGEVLGK
4	Heavy	Cysteine- and glycine-rich protein 1	P21291	GYGYGQGAGTLSTDKGESLGIKHEEAPGHRPTTN***p***NASK
5	**Heavy**	**Eukaryotic translation initiation factor 4E**	**P06730**	ATVEPETTPT***p***N***p***PTTEEEKTESNQEVANPEHYIKHPLQNR
6	Heavy	Fibronectin	P02751	LGVR***p***SQGGEA***p***REVTSDSGSIVVSGLTPGVEYVYTIQVLRDGQER,
7	Heavy	Filamin-A	P21333	AGG***p***GLERAEAGVPAEFSIWTR
8	Heavy	Heat shock cognate 71 kDa protein	P11142	RFDDAVVQSDMKHWPFMVVNDAGR***p***K, FDDAVVQSDMKHWPFMVVNDAGR***p***K
9	Heavy	Heterogeneous nuclear ribonucleoprotein A3	P51991	GFGFVTYSCVEEVDAAMCAR***p***HKVDGR
10	**Heavy**	**Homeobox protein CDX-2**	**Q99626**	KKLQQQQQQQPPQP***ppppp***Q***p***PQPQPGPLR
11	Heavy	Prosaposin	P07602	LG***p***GMADICKNYISQYSEIAIQMMMHMQPK
12	Heavy	RNA-binding motif protein, X chromosome	P38159	VEADR***p***GKLFIGGLNTETNEKALEAVFGK
13	**Heavy**	**Striated muscle preferentially expressed protein kinase**	**Q15772**	A***pp***SPGV***pp***KR
14	**Heavy**	**Trifunctional enzyme subunit beta, mitochondrial**	**P55084**	VGL***pp***LEKFNNWGGSLSLGHPFGATGCR
15	Heavy	Tubulin beta chain	Q13885	SGPFGQIFR***p***DNFVFGQSGAGNNWAKGHYTEGAELVDSVLDVVR
16	**Heavy**	**Zinc finger protein 292**	**O60281**	KSQSENV***p***ASR

Proteins were identified by liquid chromatography–tandem mass spectrometry and accession numbers and protein IDs are from the Swiss-Prot/Uniprot databases. The hydroxylated proline residue is bold, italicized, and in lower case. Peptides were filtered to 1% FDR using the Percolator algorithm in Thermo Proteome Discoverer software. Bolded (description and accession number) indicate peptides found in proteins that were not decreased in the KO.

to a decrease in mRNA. These 112 proteins were highly enriched for splicing factors, including hnRNPs, DEAD-box helicase (DDX) proteins, and other splicing factors. We therefore investigated whether OGFOD1 might alter splicing. We searched the RNA-Seq data with the mixture of isoforms (MISO) analysis software and identified 196 exon skipping events that were different in OGFOD1-KO in comparison with WT (Supplemental Table 5). One of the alternatively spliced genes was cytosolic purine 5′-nucleotidase (NT5C2), which is shown in the Sashimi plot analysis and was verified with quantitative PCR analysis (Figure 5, A and B). Interestingly, we previously found that DMOG increased exon skipping of NT5C2, which is involved in the NAD salvage pathway (17). Here, we found that the effects of DMOG on exon skipping were abolished for NT5C2 in OGFOD1-KO, which would be consistent with a role for OGFOD1 in mediating these effects on exon skipping. We performed gene ontology analysis and

Ingenuity Pathway Analysis (QIAGEN Inc.; www.qiagenbioinformatics.com/products/ingenuity-pathway-analysis/) network analysis for all the genes that were identified as being significantly different in exon skipping events between OGFOD1-KO and WT. Enriched biological processes included cell-cell adhesion, gene expression changes, and cardiac rhythm, as well as RNA splicing (Figure 5C). The top number 2 networks that were affected were "cell death and survival" as well as "RNA post-transcriptional modification, carbohydrate and nucleic acid metabolism" (Figure 5D and Supplemental Figure 3). AKT1 (also known as protein kinase B), a gene that regulates cell survival, was identified as being significantly different in exon skipping in OGFOD1-KO versus WT (Figure 5E). In the RNA posttranscriptional modification network, various forms of hnRNPs, such as hnRNPC1/C2, hnRNPD, hnRNPH1, and hnRNPK, were identified, which are all known to bind to RNA molecules with high affinity and play a role in transcription, splicing, and mRNA processing (ref. 18 and Supplemental Figure 3). Interestingly, about 50% of the proteins showing alternative splicing (Supplemental Table 5) following loss of OGFOD1 also show alternative splicing with siRNA knockdown of hnRNPA1 and DDX5 (19). Of note, DDX5 and hnRNPA1 both showed a decrease in translation in OGFOD1-KO. Liu et al. recently reported a decrease in RNA-binding proteins and splicing factors occurred with reprogramming of fibroblasts into induced cardiomyocytes (1). They further showed that polypyrimidine tract binding protein 1 (Ptbp1) inhibited the cardiomyocytes' specific splicing pattern and that Ptbp1 deletion enhanced cardiomyocyte reprogramming and enhanced expression of cardiomyocyte proteins. Interestingly, we found a significant decrease in Ptbp1 in the OGFOD1-KO cells (see Supplemental Table 1). Also of note, we found the loss of OGFOD1 altered the splicing of Ptbp1 (Supplemental Table 5).

Loss of OGFOD1 alters protein prolyl hydroxylation. To identify proteins that are highly prolyl hydroxylated specifically by OGFOD1, we searched the mass spectrometric data of OGFOD1-KO and WT for proline oxidation as a variable modification using Mascot as described in the Methods section (∑peptide spectrum matched > 2; Supplemental Figure 4). We identified 31 unique proteins (filamin-A and HSP71 were identified with both heavy and light proteins) that were prolyl hydroxylated in at least 2 of 3 WT samples but showed no prolyl hydroxylation in any of the OGFOD1-KO samples (Table 1). However, many of these proteins (those not bolded) had a decreased protein level in the OGFOD1-KO, and thus the decrease in prolyl hydroxylation measured in these proteins could just be due to the decrease in protein level (Supplemental Table 1). Alternatively, it is possible that prolyl hydroxylation of these proteins leads to their stabilization (perhaps via a protein complex) and that loss of prolyl hydroxylation leads to decreased levels. Rps23, which has been identified previously as a target of OGFOD1, was clearly identified (Table 1). Interestingly, 2 of the proteins, trifunctional enzyme subunit–β (ECHB) and cytochrome b-c1 complex subunit 1 (UQCR1), showed an increased protein level in OGFOD1-KO, and it is tempting to speculate that perhaps prolyl hydroxylation of these proteins in WT enhanced their degradation. Consistent with this premise, these 2 proteins were significantly stabilized in OGFOD1-KO.

Discussion

The α-ketoglutarate–, iron-, and oxygen-dependent superfamily of oxygenases can act as a metabolic and stress sensor. OGFOD1, a member of this family, has been shown to hydroxylate Pro62 of Rps23; however, the precise function of OGFOD1 is not fully elucidated. Inhibitors of the HIF prolyl-hydroxylase (PHD2), which are currently in clinical trials to treat anemia, have also been shown to inhibit OGFOD1 (12), adding to the importance of understanding the role of OGFOD1. This study is the first to our knowledge to examine the effect of loss of OGFOD1 in human iPSC-CMs, and the data in the study suggest the potentially novel finding that loss of OGFOD1 increases the level of cardiac sarcomeric proteins. Loss of OGFOD1 also results in a decrease in levels of Ptbp1, which has been shown to oppose the development of cardiomyocyte-specific splicing factors. Furthermore, deletion of Ptbp1 enhances expression of cardiomyocyte proteins (1). Consistent with a role for OGFOD1 in modulating cardiomyocyte differentiation, we found a rapid decrease in levels of OGFOD1 expression following addition of cardiomyocyte differentiation factors. Several recent studies have reported that changes in translation play an important role in differentiation (3, 20, 21), and consistent with this concept, we show that loss of OGFOD1 alters translation of specific proteins. It has been reported that with differentiation, large numbers of mRNAs exhibit a change in translation without a change in mRNA level (3). We found that in OGFOD1-KO iPSC-CMs, 128 proteins showed a decrease in translation; however, a decrease in mRNA was found in only 16 of the 128 proteins. Interestingly, we found that the loss of OGFOD1 resulted in a decrease in many ribosomal proteins, which could reduce total ribosome levels and further alter translation. We found that OGFOD1 loss specifically led to an alteration

in splicing factors, and alterations in splicing have emerged as an important regulator of differentiation and disease (2, 4–6, 22). A recent study shows that patients with Diamond-Blackfan anemia exhibited reduced ribosome levels in hematopoietic cells. In these cells the reduced ribosome levels selectively impaired the translation of a subset of mRNAs, thereby influencing cellular differentiation, resulting in differences in blood cell composition (23). This finding supports the general idea that alterations in ribosome levels might influence cellular differentiation processes. This study uses an iPSC model of human cardiomyocytes, which we have previously characterized and found to be immature compared with adult cardiac tissue (14). The effect of loss of OGFOD1 during development in an immature iPSC-CM could be different than in an adult cardiomyocyte.

In general, our data are consistent with previous studies showing that OGFOD1 can reduce overall translation (10). siRNA knockdown of OGFOD1 has been shown in U2OS cells to decrease proliferation, increase stress granule formation, increase phosphorylation of eukaryotic initiation factor 2 (eIF2), and decrease the overall rate of protein synthesis. However, siRNA knockdown of OGFOD1 in HeLa cells did not decrease proliferation or protein synthesis or increase stress granules or phosphorylation of eIF2 (10). Thus, the effects of OGFOD1 knockdown on these processes appears context dependent. The potentially novel finding in this study is that loss of OFGOD1 results in reduced translation of specific proteins, primarily cytoskeletal and nucleic acid–binding proteins, rather than a uniform overall reduction in translation. Previous studies as well as this study showed that OGFOD1 hydroxylates a specific proline residue on Rps23. Prolyl hydroxylation of Rps23 has been reported to be important in fidelity of mRNA translation (24). Rps23 has been shown to alter the accuracy of translation. Termination and polyadenylation 1 (TPA1), the yeast homolog of OGFOD1, has been reported to regulate termination, polyadenylation, and mRNA stability (24). The proline in Rps23, which is hydroxylated by OGFOD1, is located in the decoding region. Interestingly, alteration in decoding fidelity by other mechanisms is associated with alterations in the translation of internal ribosomal entry sites (IRESs) containing mRNAs and altered ribosomal translational activity (25). Translation of IRESs containing mRNAs has been shown to play an important role in differentiation and stem fate (20). OGFOD1, by altering the translation of key mRNAs, alters the cell proteome and leads to additional changes in protein homeostasis. Consistent with this hypothesis, mutations in Rps23, which impair OGFOD1-mediated prolyl hydroxylation of Rps23, have been shown to lead to developmental disorders (26). We further show that loss of OGFOD1 alters the translation of many ribosomal proteins, and emerging data show that ribosomal proteins can influence the mRNAs that are translated (27).

Our working hypothesis is that loss of OGFOD1 reduces prolyl hydroxylation of Rps23. As previously reported, the effects of loss of prolyl hydroxylation of Rps23 are context dependent but have been shown to include a decrease in protein synthesis. Loss of OGFOD1 and subsequent loss of Rps23 prolyl hydroxylation might alter incorporation of Rps23 into the polysome, which was shown previously (26), and the alteration in polysome composition could alter the landscape of mRNAs that are translated and could further lead to the changes in protein homeostasis that we observed. Although it is possible that OGFOD1 has additional substrates that might also contribute to the changes in protein homeostasis observed, the data could be explained by loss of prolyl hydroxylation of Rps23 upon deletion of OGFOD1. The loss of OGFOD1 decreases the translation of approximately 100 proteins, including hnRNPs, DDX proteins, and other splicing factors. We found that 50% of the proteins that showed alternative splicing (Supplemental Table 5) following loss of OGFOD1 could be explained by decreased levels of hnRNPA1 and DDX5 (19), proteins for which translation was reduced in OGOFOD1-KO. DDX5 and DDX17 both showed a decrease in translation and a corresponding decrease in protein level in OGFOD1-KO. Changes in alternative splicing have been shown to control human embryonic stem cell differentiation (2, 4, 22). Downregulated DDX5 and DDX17 have been shown to interact with hnRNPs to define epithelial and myoblast specific splicing patterns (4), and DDX5 and DDX17 are proposed to be master regulators of differentiation (4). These changes in splicing might be involved in rewiring the proteome. This concept is consistent with previous studies reporting that alterations in protein synthesis and in splicing are important in regulating cell differentiation and disease progression.

Methods

CRISPR/Cas9 knockout of OGFOD1 in iPSCs. An all-in-one CRISPR/Cas9 vector modified from pX458 (28) to enable strong Cas9 expression by CAG promoter in human iPSCs was used to express the guide RNA (gRNA) targeting OGFOD1 exon1 coding sequence (Supplemental Figure 5). The vector is available from Addgene (plasmid 79144, https://www.addgene.org/79144/). The design of the gRNA was performed by

the online CRISPR tool (http://crispr.mit.edu). iPSCs were transfected using Global Stem GeneIn reagents as described by the manufacturer. After 48 hours, GFP^+ cells were sorted using flow cytometry. The positive cells were plated at single-cell density and expanded, and the colonies were sequenced for identification of homozygous OGFOD1 knockout. To enhance OGFOD1 gRNA expression and specificity (29), gRNA sequence CGCAGGACGCCGTTCAGTCA was modified to GGCAGGACGCCGTTCAGTCA when subcloning into the CRISRP/Cas9 expression vector. Therefore, we used GGCAGGACGCCGTTCAGTCACGG (gRNA plus protospacer adjacent motif [PAM]) to search potential off-targets using the in-silico CRISPROR program (http://crispor.tefor.net) (30). The top 20 off-targets based on cutting frequency determination (CFD) off-target scores (OT1 to OT20) in parental ND2.0.6 iPSCs and OGFOD1-KO clone27 and clone33 were PCR amplified using "For" and "Rev" primers and sequenced using "Seq" primer (Supplemental Table 6). Sequence comparison showed no off-target mutations in OGFOD1-KO clones (Sanger sequencing IDs and data are shown in Supplemental Table 6). This is probably due to the fact that all of the top 20 off-targets have 4 mismatches from the gRNA sequence and low CFD off-target scores, reducing the possibility of off-target editing in selected iPSC clones. Our result is consistent with previous studies showing it was rare to find off-target mutations in TALEN- or CRISPR/Cas9–edited human pluripotent stem cells (31, 32).

iPSCs were generated from human dermal fibroblasts by reprogramming as previously described (33). Cardiac differentiation was performed following a protocol based on chemical Wnt pathway modulation as previously described (34). On day 7, after completion of the differentiation protocol, iPSC-CMs were cultured for an additional 8 days in a previously described culture medium (35).

Pulse-chase isotopic labeling with amino acids in OGFOD1-KO and WT iPSC-CMs. OGFOD1-KO and WT iPSC-CMs were transferred into light medium containing 10% dialyzed FBS (Pierce SILAC Protein Quantification Kit) for 3 days. OGFOD1-KO and WT samples were compared to the WT vehicle group, and the other group received the protein hydroxylase–inhibiting drug DMOG (1 mM, MilliporeSigma) for 6, 18, or 24 hours. For both groups, the culture medium was simultaneously switched to heavy amino acid–containing medium ($^{13}C_6$ L-lysine-2HCl, $^{13}C_6{}^{15}N_4$ L-arginine-HCl) with 10% dialyzed FBS. Samples underwent tryptic digestion. Mass spectroscopic analysis was performed using an Orbitrap Fusion. The liquid chromatography–mass spectrometry data were searched against the Swiss-Prot and UniProt databases (taxonomy *Homo sapiens* [human]) using Mascot (Matrix Science, version 2.3). Data were further analyzed with Scaffold software for quantitative proteomics.

mRNA isolation and bioanalyzer analysis. OGFOD1-KO and WT iPSC-CMs were compared to WT vehicle versus WT treated with DMOG (1 mM, MilliporeSigma) for 18 hours. mRNA isolation was performed using the RNeasy Mini Kit (QIAGEN Inc.), and the protocol was followed as described by the manufacturer. Subsequent DNAse digestion was performed with the Ambion RNA TURBO DNA-free kit as described by the manufacturer. The mRNA was purified with RNA-binding columns (RNeasy Mini Kit, QIAGEN Inc.). RNA concentrations were quantified by NanoDrop (NanoDrop ND-1000, Peglab). The purified mRNA samples were subjected to bioanalyzer analysis (Agilent RNA 6000 Nano Chip). For bioanalyzer analysis the Agilent RNA 6000 Nano Kit instructions were followed. Only high-quality samples with a calculated RNA integrity number (RIN) value of at least 8 were analyzed by RNA-Seq.

cDNA library preparation and RNA-Seq analysis. The RNA samples were processed using Illumina TruSeq Stranded Total RNA Sample Preparation kits according to the manufacturer's protocols. Briefly, RNA samples were converted into a library of template molecules of known strand origin, which were suitable for cluster generation and sequencing using the reagents provided in the Illumina TruSeq Stranded Total RNA Sample Preparation kits. First, the rRNA was removed using biotinylated, target-specific oligonucleotides combined with Illumina Ribo-Zero rRNA removal beads. After purification, RNA was fragmented into small pieces using divalent cations under elevated temperature. The cleaved RNA fragments were copied into first strand cDNA using reverse transcriptase and random primers. The products were then purified and enriched with PCR to create a final cDNA library. RNA-Seq libraries were sequenced with paired-end 50-bp reads on an Illumina HiSeq2000. The raw data in FASTQ format were aligned to human reference genome UCSC hg19 using TopHat (TopHat/2.0.13, bowtie1/2.2.3, and SAMtools/0.1.19) with the parameter –g 1 and the other options in the default settings. The refSeq transcript raw counts produced by the software rseqc/2.6 provided the input to the Bioconductor edgeR package. Trimmed mean of M values algorithms were used for normalizing the replicated samples in 2 conditions. The normalized output CPM values were compared by generalized linear model between conditions. The differentially expressed transcripts (DETs) were defined as greater than or equal to 4-fold changes with 1% FDR. The DETs were also assessed with 2-way, unsupervised hierarchical clustering analysis by computing Euclidean distance. The transcript expression

values were the log-transformed CPM reads from edgeR-normalized reads count. Alternative splicing analysis was performed using MISO (version 0.5.2; http://hollywood.mit.edu/burgelab/miso/) with settings of paired-end 120 42—read-len 50 and using –num-inc 1—num-exc 1—num-sum-inc-exc 20—delta-psi 0.30 –bayes-factor 20 for filtering events. Events were plotted with sashimi_plot function. The data are available via the National Center for Biotechnology Information's Gene Expression Omnibus database (accession number GSE130521).

Quantitative reverse transcription PCR analysis. DNAse-digested and purified mRNA samples (500 ng each) underwent reverse transcription using the iScript Reverse Transcriptase Supermix for RT-qPCR (Bio-Rad) according to manufacturer's instructions. Quantitative determination of RNA was performed by real-time reverse transcription PCR with iQ SYBR Green Supermix (Bio-Rad) according to the manufacturer's instructions. RNA18S was used as an endogenous control to normalize the quantification of the target mRNAs for difference in the amount of cDNA added to each reaction. cDNAs were diluted 1:10 with nuclease-free water and amplified using the primer pairs specific for every human sequence. Primer pair sequences were used as follows: RNA18S forward 5′-GGACATCTAAGGGCATCACAG-3′ and reverse 5′-GAGACTCTGGCATGCTAACTAG-3′, NT5C2 forward 5′-TCCTGGAGTGATCGGTTACAG-3′, and exon skipping variant reverse 5′-GTTACACTGGCTCTCCGATGA-3′ (IDT DNA). All measurements were performed with the LightCycler 96 Real-Time PCR System (Roche) and analyzed with the respective LightCycler 96 software (Roche). The amount of RNA was estimated according to the comparative Ct method with the $2^{-\Delta\Delta Ct}$ formula.

Statistics. Data were expressed as mean ± SEM. Student's *t* test (2-tailed, homodynamic variance) was used to compare between 2 groups, and 2-way ANOVA was used for multiple comparisons. Measurements were made from distinct samples. For all tests a probability value less than or equal to 0.05 was considered significant. Proteome Discoverer Software (Thermo Fisher Scientific, version 1.4) was used, and data were filtered for high peptide confidence (FDR < 1%). For label-free analysis, light and heavy peptides were quantified separately using an in-house software, QUOIL (36). Data were filtered for at least 2 peptides/protein target. For RNA-Seq analysis, the normalized output CPM values were compared by generalized linear model between conditions. The DETs were defined as greater than or equal to 4-fold changes with 1% FDR as described under *cDNA library preparation and RNA-Seq analysis*. All proteomic and RNA-Seq data will be made available on a public website.

Study approval. WT and OGFOD1-KO iPSCs were derived from de-identified human fibroblast samples, and therefore are exempt from NIH Office of Human Subjects Research Protections (OHSRP) approval.

Author contributions

AS designed and performed the experiments, analyzed the data, and drafted the manuscript. LK performed studies and edited the manuscript. YY analyzed the data and edited the manuscript. SP performed the mass spectrometry studies and analyzed the mass spectrometry data. YL analyzed the data and edited the manuscript. KLL made the CRISPR-KO cell lines. MF analyzed data and edited the manuscript. J. Zhu and MG analyzed the data and edited the manuscript. J. Zou designed the OGFOD1-KO CRISPR studies, analyzed the data, and edited the manuscript. EM designed the studies, analyzed the data, and drafted the manuscript.

Acknowledgments

This work was supported by the National Heart, Lung and Blood Institute Intramural program (Z01-HL002066).

Address correspondence to: Elizabeth Murphy, National Heart, Lung, and Blood Institute, NIH, Building 10, Room 6N248B, 10 Center Drive, Bethesda, Maryland 20892, USA. Phone: 301.496.5828; Email: murphy1@mail.nih.gov.

1. Liu Z, et al. Single-cell transcriptomics reconstructs fate conversion from fibroblast to cardiomyocyte. *Nature*. 2017;551(7678):100–104.
2. Agosto LM, Lynch KW. Alternative pre-mRNA splicing switch controls hESC pluripotency and differentiation. *Genes Dev*. 2018;32(17-18):1103–1104.
3. Blair JD, Hockemeyer D, Doudna JA, Bateup HS, Floor SN. Widespread translational remodeling during human neuronal differentiation. *Cell Rep*. 2017;21(7):2005–2016.
4. Dardenne E, et al. RNA helicases DDX5 and DDX17 dynamically orchestrate transcription, miRNA, and splicing programs in cell differentiation. *Cell Rep*. 2014;7(6):1900–1913.
5. Zhang T, et al. Rbm24 regulates alternative splicing switch in embryonic stem cell cardiac lineage differentiation. *Stem Cells*.

2016;34(7):1776–1789.
6. Gao G, Dudley SC. RBM25/LUC7L3 function in cardiac sodium channel splicing regulation of human heart failure. *Trends Cardiovasc Med*. 2013;23(1):5–8.
7. Markolovic S, Wilkins SE, Schofield CJ. Protein hydroxylation catalyzed by 2-oxoglutarate-dependent oxygenases. *J Biol Chem*. 2015;290(34):20712–20722.
8. Rose NR, McDonough MA, King ON, Kawamura A, Schofield CJ. Inhibition of 2-oxoglutarate dependent oxygenases. *Chem Soc Rev*. 2011;40(8):4364–4397.
9. Gorres KL, Raines RT. Prolyl 4-hydroxylase. *Crit Rev Biochem Mol Biol*. 2010;45(2):106–124.
10. Singleton RS, et al. OGFOD1 catalyzes prolyl hydroxylation of RPS23 and is involved in translation control and stress granule formation. *Proc Natl Acad Sci U S A*. 2014;111(11):4031–4036.
11. Wehner KA, Schütz S, Sarnow P. OGFOD1, a novel modulator of eukaryotic translation initiation factor 2α phosphorylation and the cellular response to stress. *Mol Cell Biol*. 2010;30(8):2006–2016.
12. Yeh TL, et al. Molecular and cellular mechanisms of HIF prolyl hydroxylase inhibitors in clinical trials. *Chem Sci*. 2017;8(11):7651–7668.
13. Burridge PW, et al. Chemically defined generation of human cardiomyocytes. *Nat Methods*. 2014;11(8):855–860.
14. Ulmer BM, et al. Contractile work contributes to maturation of energy metabolism in hiPSC-derived cardiomyocytes. *Stem Cell Reports*. 2018;10(3):834–847.
15. Eder A, Vollert I, Hansen A, Eschenhagen T. Human engineered heart tissue as a model system for drug testing. *Adv Drug Deliv Rev*. 2016;96:214–224.
16. Sayed N, Liu C, Wu JC. Translation of human-induced pluripotent stem cells: from clinical trial in a dish to precision medicine. *J Am Coll Cardiol*. 2016;67(18):2161–2176.
17. Stoehr A, et al. Prolyl hydroxylation regulates protein degradation, synthesis, and splicing in human induced pluripotent stem cell-derived cardiomyocytes. *Cardiovasc Res*. 2016;110(3):346–358.
18. Geuens T, Bouhy D, Timmerman V. The hnRNP family: insights into their role in health and disease. *Hum Genet*. 2016;135(8):851–867.
19. Lee YJ, Wang Q, Rio DC. Coordinate regulation of alternative pre-mRNA splicing events by the human RNA chaperone proteins hnRNPA1 and DDX5. *Genes Dev*. 2018;32(15-16):1060–1074.
20. Yoffe Y, et al. Cap-independent translation by DAP5 controls cell fate decisions in human embryonic stem cells. *Genes Dev*. 2016;30(17):1991–2004.
21. Zhang H, Dou S, He F, Luo J, Wei L, Lu J. Genome-wide maps of ribosomal occupancy provide insights into adaptive evolution and regulatory roles of uORFs during Drosophila development. *PLoS Biol*. 2018;16(7):e2003903.
22. Yamazaki T, et al. TCF3 alternative splicing controlled by hnRNP H/F regulates E-cadherin expression and hESC pluripotency. *Genes Dev*. 2018;32(17-18):1161–1174.
23. Khajuria RK, et al. Ribosome levels selectively regulate translation and lineage commitment in human hematopoiesis. *Cell*. 2018;173(1):90–103.e19.
24. Loenarz C, et al. Hydroxylation of the eukaryotic ribosomal decoding center affects translational accuracy. *Proc Natl Acad Sci U S A*. 2014;111(11):4019–4024.
25. Erales J, et al. Evidence for rRNA 2′-O-methylation plasticity: Control of intrinsic translational capabilities of human ribosomes. *Proc Natl Acad Sci U S A*. 2017;114(49):12934–12939.
26. Paolini NA, et al. A ribosomopathy reveals decoding defective ribosomes driving human dysmorphism. *Am J Hum Genet*. 2017;100(3):506–522.
27. Shi Z, et al. Heterogeneous ribosomes preferentially translate distinct subpools of mRNAs genome-wide. *Mol Cell*. 2017;67(1):71–83.e7.
28. Ran FA, Hsu PD, Wright J, Agarwala V, Scott DA, Zhang F. Genome engineering using the CRISPR-Cas9 system. *Nat Protoc*. 2013;8(11):2281–2308.
29. Fu Y, Sander JD, Reyon D, Cascio VM, Joung JK. Improving CRISPR-Cas nuclease specificity using truncated guide RNAs. *Nat Biotechnol*. 2014;32(3):279–284.
30. Haeussler M, et al. Evaluation of off-target and on-target scoring algorithms and integration into the guide RNA selection tool CRISPOR. *Genome Biol*. 2016;17(1):148.
31. Smith C, et al. Whole-genome sequencing analysis reveals high specificity of CRISPR/Cas9 and TALEN-based genome editing in human iPSCs. *Cell Stem Cell*. 2014;15(1):12–13.
32. Veres A, et al. Low incidence of off-target mutations in individual CRISPR-Cas9 and TALEN targeted human stem cell clones detected by whole-genome sequencing. *Cell Stem Cell*. 2014;15(1):27–30.
33. Beers J, et al. A cost-effective and efficient reprogramming platform for large-scale production of integration-free human induced pluripotent stem cells in chemically defined culture. *Sci Rep*. 2015;5:11319.
34. Lian X, et al. Directed cardiomyocyte differentiation from human pluripotent stem cells by modulating Wnt/β-catenin signaling under fully defined conditions. *Nat Protoc*. 2013;8(1):162–175.
35. Hirt MN, et al. Functional improvement and maturation of rat and human engineered heart tissue by chronic electrical stimulation. *J Mol Cell Cardiol*. 2014;74:151–161.
36. Wang G, Wu WW, Zeng W, Chou CL, Shen RF. Label-free protein quantification using LC-coupled ion trap or FT mass spectrometry: reproducibility, linearity, and application with complex proteomes. *J Proteome Res*. 2006;5(5):1214–1223.